AGU PUBLICATIONS

JGR

Journal of Geophysical Research: Space Physics

RESEARCH ARTICLE
10.1002/2016JA022695

Key Points:
- Strong decrease in NWC signal associated with solar eclipse of 9-10 May 2013
- The effective recombination coefficient was larger than reported in the literature
- Morlet wavelet analysis shows strong wave-like signatures associated with SEs

Correspondence to:
S. Kumar,
kumar_su@usp.ac.fj

Citation:
Kumar, S., A. Kumar, A. K. Maurya, and R. Singh (2016), Changes in the *D* region associated with three recent solar eclipses in the South Pacific region, *J. Geophys. Res. Space Physics*, *121*, doi:10.1002/2016JA022695.

Received 14 MAR 2016
Accepted 8 JUN 2016
Accepted article online 10 JUN 2016

Changes in the *D* region associated with three recent solar eclipses in the South Pacific region

Sushil Kumar[1], Abhikesh Kumar[1], Ajeet K Maurya[2], and Rajesh Singh[3]

[1]School of Engineering and Physics, University of the South Pacific, Suva, Fiji, [2]School of Electrical and Computer Engineering, Georgia Institute of Technology, Atlanta, Georgia, USA, [3]Dr. K. S. K. Geomagnetic Research Laboratory, IIG, Allahabad, India

Abstract We estimate *D* region changes due to 22 July 2009 total solar eclipse (SE), 13–14 November 2012 total SE, and 9–10 May 2013 annular SE, using VLF navigational transmitters signal observations at Suva, Fiji. The North West Cape (NWC) signal (19.8 kHz) showed an amplitude and phase decrease of 0.70 dB and 23° during November SE and 2.0 dB and 90° during May SE. The modeling using Long Wave Propagation Capability code for NWC-Suva path during November and May SEs showed an increase in average *D* region reflection height (H') and sharpness factor (β) by 0.6 and 0.5 km and 0.012 and 0.015 km^{-1}, respectively. The July total SE for JJI-Suva path showed an increase in H' of 1.5 km and a decrease in β of 0.055 km^{-1}. The decrease in the electron density calculated using SE time H' and β is maximum for July total SE and minimum for May annular SE. The effective recombination coefficient estimated from the decay and recovery of signal phase associated with May annular SE was higher (27%) than normal daytime value 5.0×10^{-7} cm^{-3} s^{-1} and varied between 1.47×10^{-6} and 1.15×10^{-7} cm^{-3} s^{-1} in the altitude 70 to 80 km. Morlet wavelet analysis of signals amplitude shows strong wave-like signatures (WLS) associated with three SEs with period ranging 24–66 min, but the intensity and duration of WLS show no clear dependence on SE magnitude and type. Apart from the cooling spot, the eclipse shadow can also generate WLS associated with atmospheric gravity waves.

1. Introduction

The major portion of solar radiation during the solar eclipses (SEs) is reduced suddenly, which produces temporal changes in the Earth's atmosphere including ionosphere [e.g., *Anderson et al*., 1972; *Antonia et al*., 1979; *Chimonas and Hines*, 1970; *Chimonas*, 1970; *Singh et al*., 1989; *Afraimovich et al*., 1998; *Clilverd et al*., 2001; *Baran et al*., 2003; *Chandra et al*., 2007; *Zhang et al*., 2010; *Chuo*, 2013; *Maurya et al*., 2014, and references therein]. Each SE is different from others in terms of their occurrence time, day and year, location of observing station, percentage of the solar disk occultation, and state of the near Earth's environment [*Baran et al*., 2003]; therefore, continuous investigations on SEs ionospheric effects, mainly in the lower ionosphere, are needed to better establish the SE effects and their variability.

Afraimovich et al. [2013] presented a review of ionospheric response to natural (including SEs) and anthropogenic processes using GPS/GLONASS radio sounding of ionosphere. The *D* region is far too high for balloons to probe and too low for satellite measurements. Radio sounding (e.g., ionosondes and incoherent radars) particularly for nighttime *D* region does not work due to its low electron density to reflect high-frequency radio waves. Therefore, the *D* region of ionosphere which ranges from 60 to 75 km in the day and 75–95 km at the night [*Hargreaves*, 1992] remains the least studied region of the ionosphere [*Cummer and Inan*, 2000]. But the very low frequency (VLF) signals generated by the lightning discharges and the VLF navigational transmitters located across the world form diagnostic tools for continuous monitoring of the *D* region ionosphere [*Clilverd et al*., 2001]. VLF waves propagate by the process of multiple reflections in the waveguide formed by the Earth (ground or sea) and the lower ionosphere called Earth-ionosphere waveguide (EIWG). The lower ionosphere is a variable upper wall of the EIWG which can be affected from top by space weather events (geomagnetic storms and solar flares) and from bottom by atmospheric wave (planetary, tidal, gravity, and infrasonic waves) [*Laštovička*, 2009; *Kumar et al*., 2015]. The supersonic motion of cooling spot of SEs in the stratosphere (ozone layer) around 45 km altitude disturbs the heat balance of the atmosphere and has been considered to be the major source of atmospheric gravity waves (AGWs) [*Chimonas and Hines*, 1970; *Chimonas*, 1970; *Gerasopoulos et al*., 2008] with the period ranging from minutes to a few hours. AGWs, whose dynamics is characterized by the interplay of buoyancy and gravitational forces, and which propagate outward and upward to ionospheric heights and can cause the traveling ionospheric

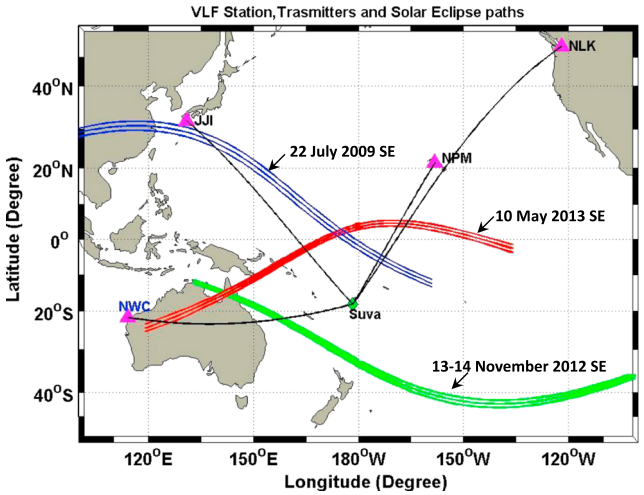

Figure 1. Map showing the positions of the VLF transmitters and the receiving station Suva. The paths of three SE totalities are also plotted.

disturbances in the ionosphere [*Vlasov et al*., 2011; *Chen et al*., 2011]. The AGWs are the strong sources of short-timescale ionospheric variability and hence can significantly change radio wave propagation conditions. The temperature and wind structures of the atmosphere determine the propagation characteristics of the AGWs. The major effects of AGWs occur in the middle atmosphere between 10 and 110 km altitudes because of decreasing density and increasing wave amplitudes with altitude. *Cheng et al*. [1992] for the SE of 23 September 1987, using phase measurements of 17.4 kHz VLF signal transmission from Yosami (34.97°N, 137.02°E), Japan, recorded at Kaojong (24.95°N, 21.15°E), Taiwan, found that AGWs were produced by the moving bow wavefront of the SE with a period between 17 and 23 min and wavelength of about 293 km. *Maurya et al*. [2014] using Morlet wavelet analysis of JJI, Japan, (22.2 kHz) signal amplitude studied periodic wave-like signatures (WLS) of period ~16–40 min associated with AGWs during total SE of 22 July 2009. However, no studies on the *D* region effects of total SE of 13–14 November 2012 and annular SE of 9–10 May 2013 could be found in the literature.

The aim of the present work is to analyze changes in the *D* region ionosphere and AGWs from the perturbations in the subionospheric VLF propagation during three different SEs; 13 November 2012 total SE using NWC, 22 July 2009 total SE using JJI and 9–10 May 2013 annular SE using NPM, NWC, and NLK VLF navigational transmitter signals, observed at Suva, Fiji. The *D* region ionospheric changes in the reflection height (H') and exponential sharpness factor (β) have been estimated using Long Wave Propagation Capability (LWPC) code for the JJI-Suva transmitter-receiver great circle path (TRGCP) for 22 July 2009, and NWC-Suva path for 13–14 November 2012 total SE and 9–10 May 2013 annular SE. The electron density (N_e) using the H' and β has been calculated for the Wait ionosphere and compared with International Reference Ionosphere (IRI) 2012 model. Using the N_e and phase change associated with 9–10 May annular SE, the SE time effective recombination coefficient (α_{eff}) has been determined. To identify the AGWs in terms of WLS associated with SEs, the Morlet wavelet analysis of signals amplitude was carried out. The hypothesis to test is that WLS period and intensity are significantly different under the different SEs.

2. Experimental Data and Brief SEs Description

VLF signals from navigational transmitters: North West Cape (NWC) (19.8 kHz), AU; NPM (21.4 kHz), Hawaii; JJI (22.2 kHz), Japan; and NLK (24.8 kHz), USA, MSK VLF transmitters are monitored at Suva, Fiji, using a vertical electric field antenna and a SoftPAL (Software-based Phase and Amplitude Logger) VLF receiver. The positions of these VLF transmitters, receiving station (Suva), and the respective TRGCPs are given in Figure 1, wherein totality paths of three SEs are also shown. The TRGCP distances are 6.69 Mm for NWC, 5.07 Mm for NPM, 7.50 Mm for JJI, and 9.43 Mm for NLK signal which fall under the medium path length (1–10 Mm) classification [*Clilverd et al*., 2001]. Here 1 min averaged amplitude and phase data obtained from the recording using GPS-based timing at time resolution of 0.1 s have been used for analysis.

The details on the 22 July 2009 total SE which was the longest SE of this century are given by *Maurya et al*. [2014]. The 13–14 November 2012 total SE occurred on the morning of 14 November at the west of the International Date Line with maximum eclipse totality on 13 November with duration of 4 min 2 s at the east of the International Date Line (http://eclipse.gsfc.nasa.gov/SEmono/TSE2012/TSE2012.html). An annular SE took place on 9–10 May 2013 with partial begin at 21:25:10 UT on 09 May with greatest eclipse intensity at 0:26:20 UT on 10 May and ended at 2:19:58 UT on 10 May.

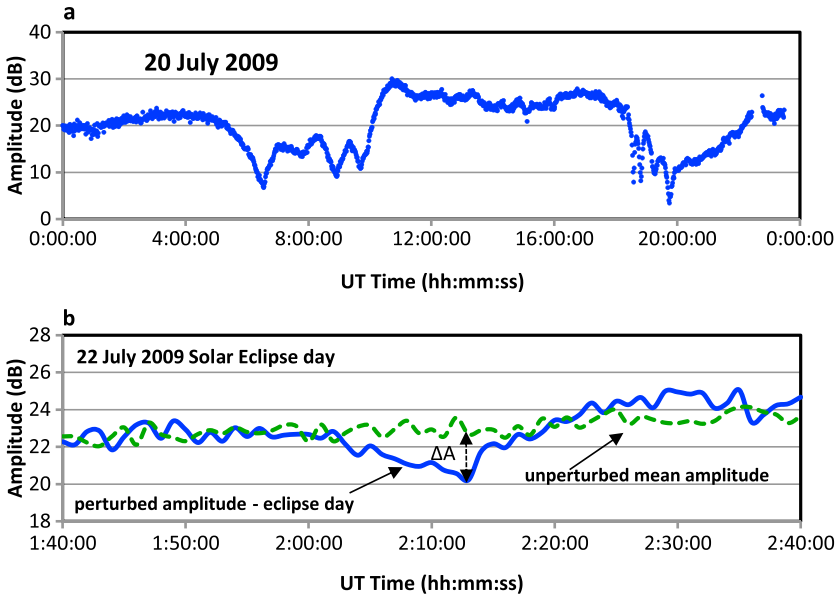

Figure 2. (a) Diurnal variation of JJI signal amplitude on 20 July 2009. (b) One hour plot of JJI signal amplitude during the SE on 22 July 2009. The amplitude on the day of the SE is plotted along with the average for two normal days (20 and 24 July). The amplitude perturbation (ΔA) of ~2.20 dB is measured from the unperturbed level (green dashed line).

3. Results

3.1. SE Associated Changes in Signals Strength

3.1.1. Total SE of 22 July 2009

Figure 2a shows diurnal variation of JJI signal amplitude for 24 h on 20 July 2009 (pre-eclipse day) at Suva. The local time (LT) of Suva is LT = UT + 12 h. There are four minima during sunrise and at least three during sunset. The sunset and sunrise minima occur during the passage of day/night terminator between the transmitter and receiver due to the destructive interference of the daytime and the nighttime modes (converted at the terminator) at the receiver. The sunrise and sunset times on 20 July 2009 at Suva at an ionospheric height of 80 km were 18:37 UT (06:37 LT) and 5:52 UT (17:52 LT), respectively. The minima during sunrise are deeper and more discrete as compared to those during sunset. The diurnal variation is driven by changes in solar zenith angle [*Thomson*, 1993] and day/night terminator movement between transmitter and receiver. The amplitude variation for 1 h period surrounding the eclipse intersection time with JJI-Suva TRGCP on 22 July total SE is shown in Figure 2b to indicate the SE effect more clearly. The amplitude values on the control day (mean of 20 and 24 July, both were magnetically normal days) have been plotted by dashed line to estimate the decrease in the amplitude (ΔA) due to the SE. The SE totality spot intercepted Suva-JJI TRGCP (Figure 1) at about 02:10 UT and JJI amplitude decreased (ΔA) by 2.2 dB with respect to unperturbed normal days averaged values. The time delay between first encounter of SE shadow with TRGCP and start of decrease in the amplitude referred to as ionospheric response time to SE was about 4 min. The average and standard deviation (σ) values of signal amplitude at the time of maximum decrease were 22.5 dB and 0.67, respectively, for 10 days of undisturbed data. Since JJI is a phase unstable transmitter, phase perturbations associated with SE could not be estimated. The value of ΔA thus measured has been used for *D* region changes associated with this SE using the Wait model.

3.1.2. Total SE of 13–14 November 2012

The 13–14 November 2012 total SE took place during geomagnetic disturbed conditions with an intense geomagnetic storm whose main phase occurred at 16:00 UT on 13 November and minimum in *Dst* index of −108 nT at 08:00 UT on 14 November (http://wdc.kugi.kyoto-u.ac.jp/). The diurnal variation of NWC signal amplitude on 14 November at Suva is shown in Figure 3a which shows three minima each during sunrise and sunset. The minima during sunset are deeper and more discrete as compared to those during sunrise. The total SE at Suva started on 13 November at around 20:05 UT and ended at 22:15 UT with eclipse magnitude of about 0.60 (www.sunearth.gsfc.nasa.gov/eclipe) during which the *Dst* index had low values varying from −13 to −25 nT. But both 13 and 14 November were geomagnetically disturbed days with ΣKp index

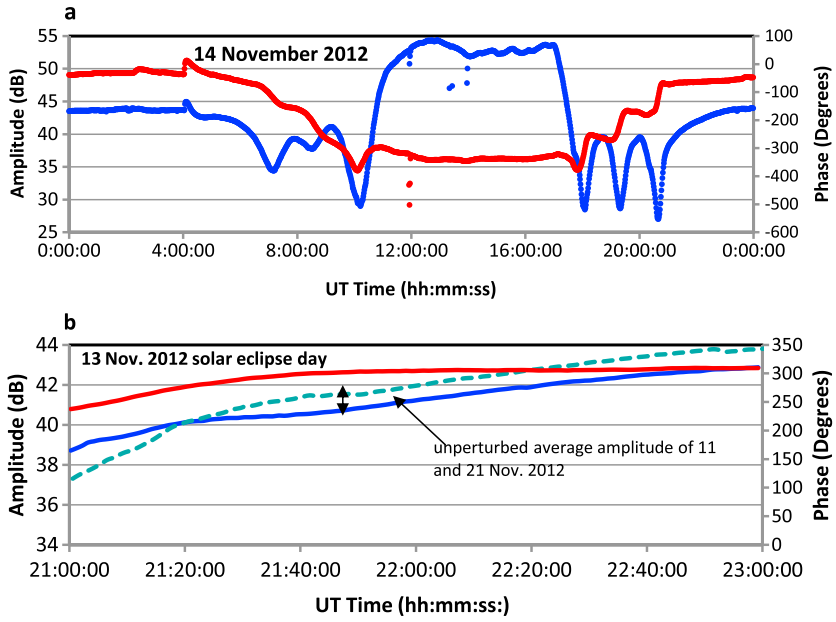

Figure 3. (a) Diurnal variation of NWC signal amplitude (blue) and phase (red) on 14 November 2012. (b) Two hour plot of amplitude and phase of NWC signal on 13 November 2012. The amplitude on the day of the SE is plotted along with the average of two normal days (11 and 21 November). The amplitude perturbation (ΔA) of ~0.70 dB is measured from the unperturbed level. The phase difference measured between the time interval 21:20–21:50 UT for the SE day on 13 November 2012 was 26° and on 11 and 21 November was 3 and 2°, respectively (not shown here).

of 26_+ and 30_-, respectively, indicating that ionosphere was in a disturbed state during the occurrence of SE. Solar obscuration reached a maximum of 55% at the time (20:55 UT) of intercept of SE with TRGCP (Table 1). The NWC amplitude variation for 2 h period on 13 November surrounding the eclipse intersection time is shown in Figure 3b to indicate the SE effect more clearly. The unperturbed amplitude values on control day (mean of 11 and 21 November, both were magnetically quiet/normal days) have also been plotted in Figure 3b, as shown by the dashed line, to estimate the decrease in the amplitude (ΔA) due to eclipse. The SE totality intercepted Suva-NWC TRGCP (Figure 1) at about 21:12 UT on 13 November and amplitude decreased (ΔA) by 0.7 dB with respect to the unperturbed SE values on control day. The σ value at the time of maximum decrease in the amplitude was 0.27 with the mean signal amplitude of 41.52 dB for 10 days of undisturbed data. This indicates that the decrease in the amplitude was more than 2σ. The decrease in the amplitude started at 21:25 UT and maximum decrease in the amplitude occurred at 21:46 UT giving a *D* region ionospheric response time of about 13 min between the SE totality spot encounter with TRGCP and start of decrease in the amplitude. The NWC is a phase stable transmitter and reproduces almost the same pattern over the days, but the phase increases over the days. The phase perturbations associated with this SE were estimated by measuring the phase difference in the time interval 21:20–21:50 UT on 13 November minus the phase difference on control day and 10 other randomly selected days for the same time

Table 1. The Details of Solar Eclipses and Associated Percentage Decrease in the Electron Density Estimated, Features of Wave-Like Signatures, and Distance of Cooling Spot Interaction With Path From Suva Station[a]

Event	Solar Obscuration (%)	SE Magnitude (%)	Zenith Angle (deg)	Decrease in Electron Density (%)	WLS Period and Duration	Cooling Spot Interaction Distance From Station
22 July 2009	44.5	54.0	70.7	25.5	24–60 min 01:15–03:30 UT	JJI path 6678 km
13 Nov 2012	55.0	63.2	40.4	32.9	40–66 min 21:24–22:42 UT	NWC path 2449 km
10 May 2013	30.9	42.8	35.7	16.5	20–66 min 00:00–02:24 UT	NPM path 2783 km

[a]22 July 2009 SE [*Maurya et al.*, 2014].

interval. The phase decrease on 13 November in the time interval 21:20–21:50 UT of SE was 26° and average phase variation for this duration on control day was 3° giving a phase decrease of 23° associated with the SE. Similar (about 3°) phase build was also seen during 21:20–21:50 UT on 10 other normal days.

3.1.3. *Annular SE of* 9–10 May 2013

The 9–10 May 2013 annular SE occurred during very quiet geomagnetic conditions where *Dst* had mostly positive values with a little variation and *Kp* varied between +1 and −1 (http://wdc.kugi.kyoto-u.ac.jp/). This annular eclipse path while starting to trace the globe first crossed the NWC-Suva TRGCP (medium length path) near the transmitter while the eclipse shadow traveled along the TRGCP before crossing it. Solar obscuration reached a maximum of 31% at the time of intercept of SE with TRGCP (Table 1). Two hour plots of amplitude (blue) and phase (red) of NWC signal in the interval 22:00–00:00 UT on 9 May is shown in Figure 4a. The amplitude perturbation (ΔA) of ~0.7 dB with respect to the unperturbed normal values on control day (mean of 10 and 11 May, both were magnetically quiet days) was estimated. The σ value at the time of maximum decrease in the amplitude was 0.25 with the mean signal amplitude of 37.6 dB for 10 days of undisturbed data. The phase perturbation ($\Delta\phi$) of ~ 90° was measured with respect to the mean unperturbed phase. The phase was stable on 09–11 May and did not build up which allowed us to estimate the $\Delta\phi$ from the mean unperturbed value as shown in Figure 4a.

The 9–10 May annular SE also perturbed the transmissions from NPM and NLK transmissions received at Suva. The diurnal variation of NPM signal amplitude and phase on 11 May 2013 is shown in Figure 4b. The NPM signal propagates across the geomagnetic equator over the sea largely in north-to-south direction and comparatively less in east-to-west direction. The signal minima are not as distinct as in the case of JJI and NWC signals; however, a minimum each during both sunrise and sunset transitions can be seen. The annular SE of 9–10 May 2013 first intercepted the NPM-Suva TRGCP at around 22:40 UT on 9 May with shadow arriving at Suva and cooling spot interacted with path at 01:33 UT on 10 May and ended at 03:25 UT on 10 May with eclipse magnitude of about 0.45 (www.sunearth.gsfc.nasa.gov/eclipe). The amplitude variation for 2 h period on 10 May surrounding eclipse interception time with TRGCP is shown in Figure 4c to indicate the SE effect more clearly. The amplitude values on control day (mean of 11 and 12 May) have been plotted in Figure 4c as shown by dashed curve to estimate the decrease in the amplitude (ΔA) due to this eclipse. The partial SE on 10 May was at its greatest when it crossed the NPM-Suva TRGCP around 01:25 UT and the NPM amplitude decreased (ΔA) by 2.0 dB with respect to the unperturbed control day value. The values of σ and mean amplitude at the time of maximum decrease were 0.56 and 38.9 dB, respectively, using 10 days of undisturbed data. The decrease in the amplitude started at 01:35 UT and maximum decrease in the amplitude occurred at 01:52 UT giving a *D* region ionospheric response time of ~10 min between the SE first encounter with TRGCP and start of decrease in the amplitude. NPM is a phase stable transmitter, but no phase perturbation associated with this eclipse could be identified. Similar effect of this annular eclipse was also seen on the NLK signal on 10 May at around 01:40 UT when the eclipse path first passed over the NPM-Suva TRGCP and later intercepted NLK-Suva TRGCP. The NLK signal amplitude variation for 2 h period during 10 May surrounding eclipse interception time with TRGCP is shown in Figure 4d. The values of amplitude on control day (9 and 11 May) have also been plotted in Figure 4d as shown by dashed curve to estimate the decrease in the amplitude (ΔA) due to this eclipse. A maximum amplitude decrease of about ~ 1.8 dB was measured with respect to the unperturbed mean value at 02:00 UT. The σ value at the time of maximum decrease in the amplitude was 0.71 with the mean signal amplitude of 21.2 dB for 10 days of undisturbed data. A time difference (*D* region ionospheric response) of ~4 min was measured between the first encounter of the SE with the TRGCP at the time 01:40 UT and when the amplitude started showing its decrease at 01:44 UT. No significant phase perturbation was apparent.

3.2. *D* Region Changes Associated With SE

The *D* region ionosphere up to the altitude of 100 km in its simple form can be characterized by the reference height *H*′ (km) and the exponential sharpness factor β (km^{-1}) parameters [*Wait and Spies*, 1964]. The parameters *H*′ and β control the altitude profile and the sharpness of the *D* region electron density, respectively. The modeling of the amplitude decrease in JJI signal strength by 2.2 dB associated with 22 July 2009 total SE gives perturbed values of *H*′ and β as 72.0 km and 0.340 km^{-1}, respectively, as compared to unperturbed values 70.3 km and 0.395 km^{-1} as estimated from LWPC V2.1 modeling shown in Figure 5. In order to accurately model the *D* region using LWPC, it is better to have both the amplitude and phase perturbation data.

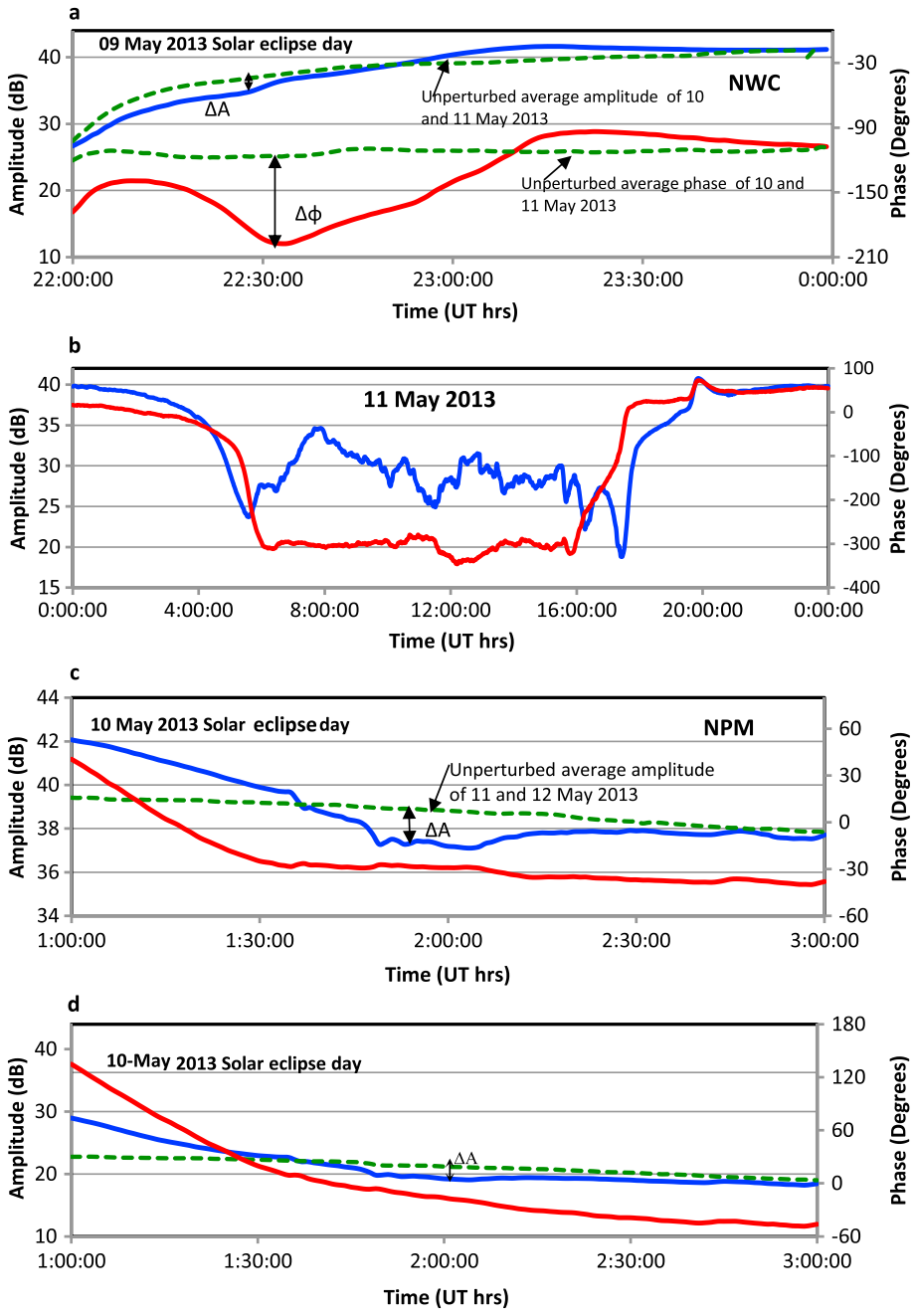

Figure 4. (a) Two hour plot of amplitude (blue solid curves) and phase (red solid curves) of variations of NWC signal on 9 May 2013. The amplitude perturbation (ΔA) of ~0.70 dB and perturbation ($\Delta\phi$) of 90° is measured from the unperturbed level (green dashed line). (b) Diurnal variation of NPM signal amplitude (blue) and phase (red) on 11 May 2013. (c) Two hour plot of amplitude (blue) and phase (red) of NPM signal on 10 May 2013. The amplitude perturbation (ΔA) of ~2.0 dB is measured from the unperturbed level (green dashed line). The eclipse was at its greatest when it crossed the NPM-Suva TRGCP around 01:50 UT. The phase perturbation is not evident. (d) Two hour plot of amplitude (blue) and phase (red) of NLK signal on 10 May 2013. The amplitude perturbation (ΔA) of ~1.8 dB is measured from the unperturbed level (green dashed line).

Therefore, the SE of 13 November 2012 showing a NWC signal phase decrease of 23° along with the amplitude decrease of 0.7 dB was modeled for the *D* region parameter changes using LWPC V2.1 code. The *D* region parameters during SE for the unperturbed daytime ionosphere for the NWC-Suva path were estimated as $H' = 70.5$ km and $\beta = 0.390\ \mathrm{km}^{-1}$ using the polynomial equations for H' and β as a function of solar zenith angle given by *McRae and Thomson* [2000]. By adjusting the values of H' and β to match the

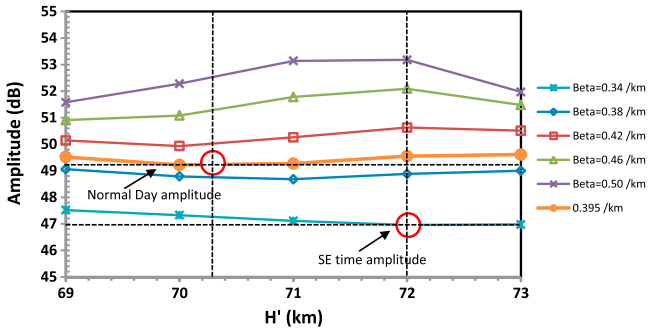

Figure 5. *D* region parameters (H', β) estimated for the JJI to Suva path using LWPC VLF amplitude modeling for the 22 July 2009 total SE. The horizontal dashed (black) lines show the normal day time and SE time JJI amplitudes and their points of intersection (shown by red circles) with plots give the value of β. The vertical dashed lines intersecting with plots and amplitude lines give corresponding values of H'.

values of perturbed amplitude and phase during the SE, the estimated perturbed values are $H' = 71.1$ km and $\beta = 0.402\ \mathrm{km}^{-1}$. This gives an average increase in H' of 0.6 km and an increase in β of $0.012\ \mathrm{km}^{-1}$. Similarly, during 09 May 2013 annular SE for NWC-Suva path, the unperturbed daytime ionospheric values of H' and β are 70.5 km and $0.390\ \mathrm{km}^{-1}$, and SE perturbed values of $H' = 71.0$ km and $\beta = 0.405\ \mathrm{km}^{-1}$ have been obtained. Since the single electron density profile cannot be applied for the entire path and and SE did not affect the entire path and uniformly, this increase in H' and β is not the uniform increase in the SE-affected part of TRGCP rather is an average increase in H' and β along the entire path that would have produced the same phase and amplitude perturbations.

The *D* region electron density height profiles $N_e(h)$ in cm^{-3} have been constructed using the Wait profile [*Wait and Spies*, 1964] both for unperturbed and SE perturbed conditions given as

$$N_e(h) = 1.43\times10^{7}[\exp(-0.15H')\ \exp[(\beta - 0.15)(h - H')]. \quad (1)$$

Several researchers have used this conventional Wait profile (equation (1)) to determine the *D* region electron density under the normal conditions and disturbed conditions due to solar and geomagnetic activities [e.g., *McRae and Thomson*, 2004; *Thomson et al*., 2005; *Kumar et al*., 2015]. This electron density profile (equation (1)) gives a simple effective average change during the SEs along the TRGCPs; however, a more realistic *D* region profile using the technique given by *Todoroki et al*. [2007] could also be determined. Using equation (1), we have shown in Figure 6 the $N_e(h)$ in the altitude range of 65–80 km using unperturbed ($H' = 70.5$ km and $\beta = 0.390\ \mathrm{km}^{-1}$) and perturbed ($H' = 71.1$ km and $\beta = 0.402\ \mathrm{km}^{-1}$) daytime ionosphere for 13 November 2012 SE and 9 May 2013 perturbed ($H' = 71.1$ km and $\beta = 0.402\ \mathrm{km}^{-1}$) for NWC-Suva path. For 13 November 2012 SE, N_e at the daytime reflection height of 75 km decreased to $8.92\times10^{2}\ \mathrm{cm}^{-3}$ from the normal daytime value of $1.075\times10^{3}\ \mathrm{cm}^{-3}$ giving 17.0% reduction in N_e. For 9 May 2013 SE, N_e at the daytime reflection height of 75 km decreased to $9.39\times10^{2}\ \mathrm{cm}^{-3}$ from the normal daytime value of $1.075\times10^{3}\ \mathrm{cm}^{-3}$ giving 12.6% reduction in N_e. The N_e reduction under the total SE of 13–14 November 2012 is more when compared with that due to the annular SE of 9–10 May 2013. Again, this is not a reduction in the N_e in the SE-affected portion of TRGCP rather is an average decrease in N_e along the entire TRGCP. The N_e profile has also been obtained using the IRI 2012 model for the location of Suva for SE on 9 May at 22:30 UT (10:30 LT) and

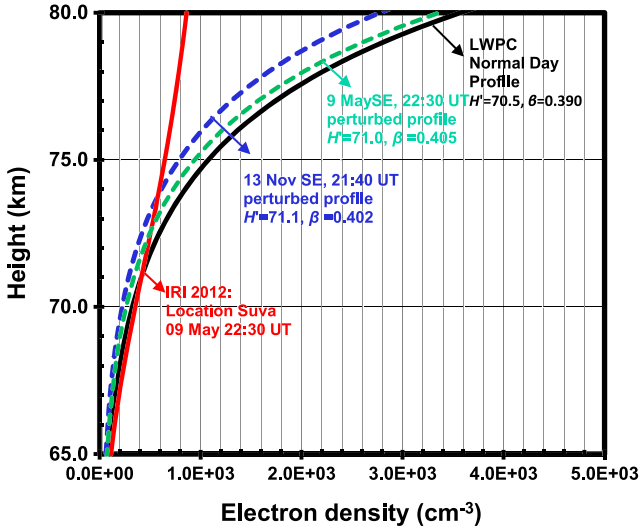

Figure 6. Electron density profiles determined by LWPC VLF modeling during 13 November 2012 annular SE (blue color dashed line) and 9 May 2013 (green dashed line) total SE. The normal unperturbed electron density profile on 9 May at 22:30 UT (10:30 LT) is shown using the LWPC model (black solid line) and IRI 2012 for the location of Suva station.

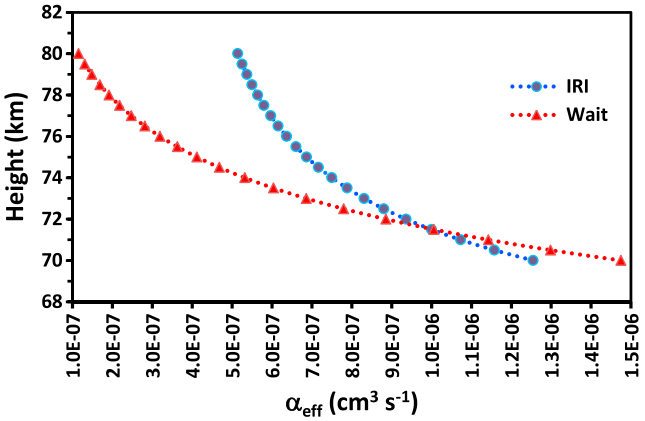

Figure 7. Vertical profile of the effective recombination coefficient (α_{eff}) during annular SE day of 9 May 2013 at 22:30 UT (10:30 LT) for Suva using *Wait and Spies* [1964] and IRI 2012 electron density profiles.

is shown in Figure 6 (red line). The IRI 2012 model shows N_e equal to 6.45×10^2 cm^{-3} at the 75 km height which is 40% less than that obtained from LWPC modeling at this height. The difference in IRI and LWPC determined N_e increases as we move above the 72 km height below which there seems good agreement between both the models.

The electron density of the *D* region for normal days is proportional to $\sqrt{F\cos\chi}$, where F is solar flux and χ is solar zenith angle which during eclipse day decreases to where γ is obscuration rate of Sun during the eclipse event [*Ratnam et al.*, 2012]. The average electron density decrease of 26, 33, and 17 percentages is estimated for July, November, and May SEs (Table 1) for which solar obscurations were 45, 55, and 31 percentages, respectively. The decrease in electron density as given in Table 1 is not specific along any TRGCP shown is Figure 1 rather is the general decrease in the electron density by SEs and depends upon type and magnitude of SE.

The effective recombination coefficient (α_{eff}) at various daytime *D* region heights can be estimated [*Mitra*, 1968, 1974] using the phase decay curve for solar flare or solar eclipse conditions. The α_{eff} using phase variation associated with SEs both during decay and recovery times, assuming ionospheric response to be time independent over the duration of SE effect [*Lynn*, 1981], is determined using the relation

$$\alpha_{eff} = \frac{|1 - \varnothing_2/\varnothing_1|}{N_e|(t_2 - t_1)|} \tag{2}$$

where ϕ_1 and ϕ_2 are phase changes at times t_1 and t_2, respectively, during the decrease in the phase and N_e is the electron density at the normal daytime reflection height (75 km taken here). The 9–10 May 2013 SE has shown a very systematic decrease in phase which we have used to estimate the α_{eff}. We measured the phases (ϕ_1 and ϕ_2) at every 5 min interval ($t_2 - t_1$) at 5 points each for decay and recovery of the phase shown in Figure 4a which have been used to calculate the α_{eff}. The average value (10 points) of α_{eff} comes out to be 5.59×10^{-7} cm^{-3} s^{-1} at 75 km (normal reflection height) and 1.56×10^{-7} cm^{-3} s^{-1} at 80 km. The value of α_{eff} is larger by 24% to the daytime ionospheric quiescent condition value of $\alpha_{eff} = 4.5 \times 10^{-7}$cm^{-3} s^{-1} [*Mitra*, 1968] but small compared to nighttime value of [*Belrose et al.*, 1964]. Using the IRI 2012 model for the location of Suva for SE on 9 May at 22:30 UT (10:30 LT), we found N_e to be 6.45×10^2 cm^{-3} at the 75 km height which is 23.4% less than that obtained using LWPC modeling at the same height. Considering SE time reduction of 12.6% in IRI given N_e, and using equation (1), the value of α_{eff} comes out to be 6.86×10^{-7}cm^{-3}s^{-1} at 75 km (normal reflection height) and 5.14×10^{-7} cm^{-3} s^{-1} at 80 km. The vertical profile of α_{eff} in the altitude range of 70–80 km during SE time using both Wait model and IRI model N_e is shown in Figure 7.

3.3. Wavelet Analysis of Signal Amplitude During SEs

Wavelet transform-based methodology to detect AGW packets (or structures) propagating up to ionospheric heights has been used by several researchers [e.g., *Sauli et al.*, 2006, and references therein]. For the detection and characterization of acoustic waves, Morlet mother wavelet is preferred over Paul mother wavelet [*Sauli et al.*, 2006]. To determine the wave-like signatures (WLS) due to AGWs associated with SEs, the Morlet mother wavelet analysis, as used by *Maurya et al.* [2014] for the 22 July total SE, has been carried out of NWC amplitude signal during13–14 November 2012 total SE and for NPM signal amplitude during 9–10 May 2013 annular SE, with the aim of finding the changes in the gravity waves characteristics associated with different SEs. In order to find out eclipse associated WLS, we have subtracted normal day VLF signal amplitude values from instantaneous values on the eclipse day for the respective eclipses. Further, we applied wavelet analysis with 20–80 min period range Butterworth band-pass filter to the subtracted amplitude data

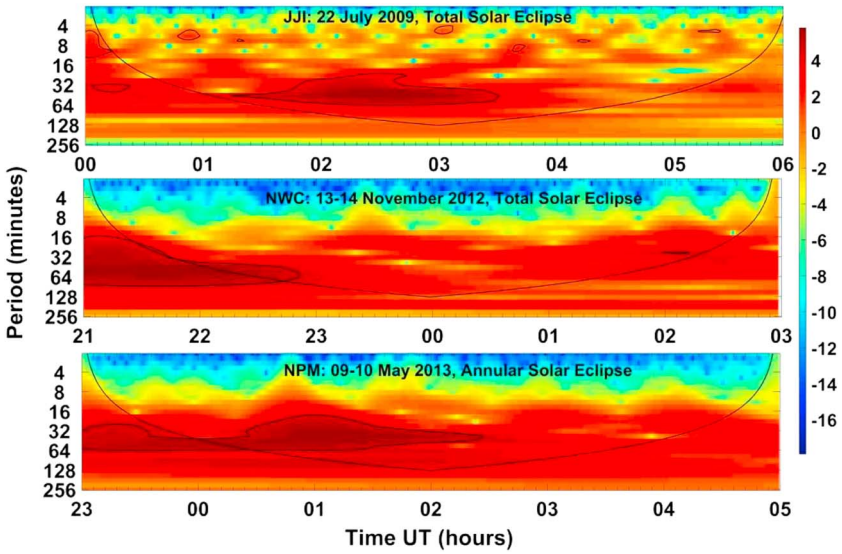

Figure 8. The wavelet spectra based on the Morlet wavelet analysis of JJI, NWC, and NPM signal filtered amplitude observed during 22 July 2009 total SE [*Maurya et al*., 2014], 13–14 November 2012 total SE, and 9–10 May 2013 annular SE day for 6 h duration at each station. The black thick contours show 95% confidence line of the period, and the bowel shape contours show the cone of influence; anything below is dubious. Hence, the period lying between these two curves is significant. The intensity of WLS on arbitrary scale is shown by the color column.

for these partially eclipsed stations to focus on short-term oscillations associated with AGWs during SEs and to look at lower side of WLS period than that studied by *Maurya et al*. [2014] using 30–80 min period range filter. The results are shown in Figure 8 using 6 h of data surrounding eclipse time. The black thick contours show 95% confidence line of the period, and the bowel shape contours show the cone of influence; anything below is dubious. The results on WLS are also summarized in Table 1. The distance between the cooling spot interaction with TRGCPs from receiving station Suva was 6678 km for 22 July 2009 total SE on JJI path, 2449 km on NWC path for 13–14 November 2012 total SE, and 2783 km on NPM path for 9–10 May 2013 annular SE. For 22 July 2009 total SE the WLS with period of 24–60 min occurred during 01:15 to 03:30 UT. The eclipse effect was due to SE shadow intercepting JJI-Suva TRGCP near the transmitter with a delay of ~55 min between the first encounter of SE shadow with TRGCP and start time of WLS. Within the contour of cone of influence in Figure 8 (top), there appear a couple of events of short duration comparatively weaker WLS with the periods of few minutes (below the lower period cutoff of the filter) which could be associated with acoustic waves. For 13–14 November 2012 total SE, we have selected data starting at 21:00 UT on 13 November to 03:00 UT on 14 November in order to avoid night/day terminator effect which itself is a strong source of gravity waves [*Nina and C˘adze*, 2013]. It can be seen that there were significant WLS present during the eclipse time (21:24 to 22:42 UT) with period of 40–66 min which may also be due to SE or solar terminator as the SE occurred during the signal buildup after the terminator passage. For 9–10 May 2013 total SE, we have selected NPM transmitter for the analysis since NWC-Suva TRGCP was mostly during dark and terminator transition, and NLK was not affected by the SE. For NPM-Suva path, we see the presence of strong WLS with period ~20–66 min during ~ 00:00 UT–02:24 UT on 10 May. The time of occurrence of WLS indicated that they occurred about 80 min after eclipse commencement (22:40 UT) at Suva. The cooling spot intercepted NPM-Suva TRGCP about 2 h after the SE shadow touched Suva. We do not see any dependence of type and magnitude of SEs on WLS period, duration, and intensity of WLS (Table 1 and Figure 8).

4. Discussion

The *D* region ionospheric changes due to sudden decrease in the solar radiation associated with total SEs on 22 July 2009 and 13–14 November 2012 and an annular solar eclipse on 9–10 May 2013 have been studied. The total SEs on 22 July 2009 and 13 November 2012 were followed by moderate and intense storms, respectively; however, the geomagnetic disturbances during these SEs were not strong enough to produce any noticeable effect on the low-latitude *D* region ionosphere [*Peter et al*., 2006; *Kumar and Kumar*, 2014].

The *D* region effects of 22 July 2009 SE effects particularly in the Indian and Chinese sectors using ELF-VLF signals have been studied by several researchers [*Guha et al*., 2010; *Singh et al*., 2011; *Zhang et al*., 2011; *Ohya et al*., 2012; *Pal et al*., 2012; *Phanikumar et al*., 2014; *Maurya et al*., 2014]. We have primarily used 22 July SE data [*Maurya et al*., 2014] for modeling the *D* region ionosphere for JJI-Suva path and comparing periodic WLS associated with 12 November 2012 and 9 May 2013 SEs. The *D* region ionospheric response time of ~4–13 min estimated between the first encounter of three SEs with respective TRGCPs and start of decrease in the amplitude is consistent with observations by *Clilverd et al*. [2001] but are shorter than the response times (~1–2 h) found by several researchers [*Altadill et al*., 2001; *Zhang et al*., 2010; *Yadav et al*., 2013] for SEs effect in the *E* and *F* region ionosphere.

During SEs, sudden short-lived decrease in solar flux creates nighttime-like situation with maximum effect in the shadow region which decreases both the sides of shadow and changes the normal physical and chemical processes of the *D* region. The totality shadow has major blockage of Lyman α radiation which under normal daytime is mainly responsible for the major *D* region ionization. But electron density in the SE region is still higher than the pure nighttime conditions due to some ionization produced by limb solar corona originated EUV and soft X-ray radiations [*Curto et al*., 2006; *Singh et al*., 2011]. The discontinuity created by the eclipse region in the TRGCPs causes the changes in the VLF propagation conditions giving a net increase or decrease in the VLF signal amplitude and phase at the receiving station. The blockage of Lyman α (1215 Å) by the Moon during SEs decreases the ionization process and increases the recombination in the ionosphere including *D* region ionosphere. The SE-associated decrease of ionization leads to the perturbations in ionospheric electron density and electrical conductivity and drives the *D* region upward according to the decrease in the radiation along the TRGCP. Since the entire TRGCP was not affected uniformly by SEs, the *D* region VLF reflection height decreases will be different at different locations of the TRGCP affected by SE. Therefore, the reflection height estimated at any station is the path-integrated reflection height. Using tweek sferics recorded at Allahabad (geographic latitude, 25.40°N) and Nainital (geographic latitude, 29.35°N) during 22 July 2009 total SE effect, *Singh et al*. [2011] calculated tweek (VLF) reflection height and found a gradual increase/decrease in the tweek reflection height/*D* region electron density with the progress/decay of eclipse magnitude at both stations. The increase in the tweek reflection height of about 5–8 km in the Indian region was estimated by *Guha et al*. [2010] and *Singh et al*. [2011] associated with SE of 22 July 2009. The observations of Indian Transmitter (VTX) signal (18.2 kHz) for the path length of 2000 km and more in the northeastern part of India showed a decrease in the signal amplitude for 22 July 2009 total SE [*Guha et al*., 2010; *Pal et al*., 2012]. Our results for 13–14 November 2012 total SE for the NWC-Suva path show that NWC signal amplitude and phase decreased by about 0.70 dB and 23°, respectively. For 9–10 May 2013 SE, NWC signal amplitude and phase decreased by about 0.70 dB and 90°, respectively, NPM amplitude decreased by 2.0 dB, and NLK amplitude decreased by 1.8 dB from unperturbed level. Our results of decrease in the VLF amplitude for all three SEs for medium length paths are consistent with previous studies by *Clilverd et al*. [2001] who for 11 August 1999 SE found a decrease (negative) in VLF amplitude for long paths but an increase (positive) in VLF amplitude for majority of short paths. The amplitude decrease associated with 13 November 2012 and 9 May 2013 SEs of about 0.7 dB falls within the daytime day-to-day variability of signal amplitude during the period of SEs occurrence but the phase perturbations of 26° and 90° respectively, are much larger than the day-to-day variation of phase which is within 2–3° over 2 h period on normal days. In all the cases the ΔA value was higher than at least 2σ value of the signal amplitude about the mean, further ruling out the possibility of ΔA within day-to-day variability of the signal strength at the time of the signal dip during SEs. Therefore, we believe that the amplitude decrease associated with phase decrease is really due to SEs. The complex constructive/destructive interference of modes at the receiver but generated at the SE discontinuty of decreased VLF reflection height by SE results in a net VLF signal amplitude increase/decrease to which total TRGCP length and direction, topography of receiver site, SE, and ionospheric conditions along the path also contribute [*Clilverd et al*., 2001]. Since ionizing radiations of the Sun are progressively cut off by the Moon's shadow as the eclipse progresses, the electron density in the *D* region is depleted causing the progressive increase in the VLF reflection height and hence the phase decrease. The increase in the effective VLF reflection height is due to an increase/decrease in the recombination coefficient/electron density and altitude redistribution of the ionospheric *D* region electron density due to movement of SE shadow through the ionosphere. The SEs create a discontinuity in the TRGCP due to the movement of shadow and a sharp decrease in the electron density along the movement of totality shadow and slow decrease in electron density in the

region of partial SE strength according to the strength of partiality. This increases both the parameters H' and β differently along the TRGCPs, but their path-integrated increase can be calculated using the method suggested by *Clilverd et al*. [2001] and LWPC code. The modeling of both amplitude and phase decrease associated with 13–14 November 2012 SE on NWC-Suva path using LWPC code shows that eclipse time values of H' and β were increased by 0.6 km and 0.012 km^{-1}, respectively, from the normal unperturbed values of $H' = 70.5$ km and $\beta = 0.390$ km^{-1}. The electon density N_e (h) calculated using perturbed values of $H' = 71.1$ km and $\beta = 0.402$ shows a decrease in N_e (h) which at 75 km is about 12.6% (Figure 7). Almost similar change in the unperturbed daytime ionosphere values of $H' = 71.0$ km and $\beta = 0.405$ km^{-1} have been obtained for 9–10 May 2013 SE. *Guha et al*. [2010] during the total SE of 22 July 2009 recorded the JJI transmitter signal (location, 8.38°N, 77.75°E) at Tripura station (23.75°N, 91.25°E) having a medium path with TRGCP of 2200 km. Using the method suggested by *Clilverd et al*. [2001] which states that a 1 dB increase in the amplitude and a 10° decrease in the phase results in an increment of H' by 1.1 km and β by 0.01 km^{-1}, they found increase in both H' and β to 74.5 km and 0.433 km^{-1} compared to unperturbed ionosphere values of 71 km and 0.43 km^{-1}, respectively, giving an increase in H' and β by 3.5 km and 0.003 km^{-1}, respectively. However, we cannot use the criterion of *Clilverd et al*. [2001] because it is suitable only for short paths (0–1000 km), whereas all the paths (>5000 km) under this study fall under higher side of medium lenght path (1000 km–10,000 km). *Phanikumar et al*. [2014] analyzed JJI signal received at Busan, a very short path (~390 km), during 22 July 2009 SE, and estimated an increase in H' and β to 77 km and 0.485 km^{-1}, respectively, from normal daytime values. The decrease in the amplitude and associated increase in the D region parameters indicate that the change in signal strength and the H' depends upon the path length from the point of intersection of SE shadow to TRGCP; the larger the distance less is the effect due to more mixing of modes with the distance. The ionospheric response to a SE is generally nonlinear [*Lynn*, 1981], although some authors have considered it to be linear. The parameters H' and β during SEs vary with time, distance from the transmitter, and varying amount of solar obscuration along the TRGCP. Since the entire TRGCP is not affected uniformly by the SEs, the SE time H' and β estimated here using LWPC code indicate the average change in their values along the entire path that would produce the same amplitude and D region change as observed here.

In the D region, the electrons are dominantly lost due to effective recombination which includes the dissociative recombination, mutual ionic recombination, electron to negative ion ratio and other dust capture coefficients of aerosol. During a SE, the electron production rate decreases and dissociative recombination increases resulting in corresponding decrease in the electron density. The dissociative recombination is predominant in the upper D region during the SEs and nighttime. The SE time value of α_{eff} estimated for 9 May 2013 annular SE was $6.86 \times 10^{-7} cm^{-3} s^{-1}$ at 75 km and 5.14×10^{-7} cm^{-3} s^{-1} at 80 km obtained using the IRI model with application of 12.6% decrease in N_e over LWPC values associated with 9–10 May annular SE. The α_{eff} is larger than the daytime (75 km altitude) ionospheric quiescent condition value, small compared to nighttime value, and large (~27%) compared to eclipse time value of $\alpha_{eff} = 5 \times 10^{-7}$ cm^{-3} s^{-1} at the VLF reflection height [*Grubor and Šulić*, 2002]. In this study, TRGCPs fall under medium length path (NWC-Suva path), SE is annular, and the entire path was not under SE uniformly, therefore, value of α_{eff} we have estimated is the average value of effective recombination coefficient integrated long the entire path. The α_{eff} particularly during SEs and solar flares is still poorly known and requires further investigations.

The AGW sources in the ionosphere can be earthquakes [*Molchanov and Hayakawa*, 2008], volcanic eruptions, tornadoes, thunderstorms, solar eclipses, terminators, jet flows, polar and equatorial electrojets, meteors, strong explosions, and powerful rocket launches [*Kaladze et al*., 2008]. AGWs consist of relatively high-frequency acoustic and low-frequency internal gravity waves and have typical periods from 10^2 s to about a day. AGWs can exist from the troposphere up to altitudes of 500 km, covering the entire ionosphere. The acoustic waves in atmosphere can be emitted only by supersonic motion [*Kato et al*., 1977] of the totality/annularity footprint (cooling spot) of the SEs. *Walker et al*. [1991] using the ionosonde sounding of virtual heights presented first experimental evidence of the existence of gravity waves with periods of 30–33 min in the ionosphere during the SE of 18 March 1988 in East Asia. The summary of WLS features during three different SEs for three different VLF transmitter signals recorded at Suva is presented in the Table 1 and compared with the solar obscuration, SE magnitude, solar zenith angle, decrease in the electron

density, and distance of SE interaction with TRGCP from the station. For 22 July 2009 the WLS of 22–60 min period occurred about 60 min after the eclipse start time near the transmitter. The couple of WLS events of short durations and short periods (few minutes) in Figure 8 (top) appear to be associated with the acoustic waves which could also be generated by strong lightnings around the TRGCP. For example, there were several lightnings seen in the World-Wide Lighting Location (www.wwlln.net) data (e.g., at 00:41:24.125459 UT, 32.6825°N, 134.4355°E) around the JJI transmitter location (32.040°N, 130.810°E) within 5–10 min prior to the occurrence of first short period WLS event around 00:47 UT. But it is difficult to exactly identify which lightnings were responsible for these events due to large time delay between acoustic-gravity wave generation in the troposphere and its effect on the *D* region. The intensity of these WLS events is comparatively weaker mainly due their atmospheric absorption (due to viscosity and heat conductivity) and response of the filter to the period outside its band-pass range. *Saulia et al*. [2007] have shown an acoustic wave event during total solar eclipses of 11 August 1999 with 1 min vertical profiles of electron concentration measurements at the European midlatitude ionospheric station Pruhonice (Czech Republic; 49.9°N, 14.6°E). However, the signal amplitude/electron concentration data at lower sampling rate than 1 min will give better detection of such waves. For 13 November 2012 SE event, we see significant WLS on NWC signal during the 21:00–22:40 h UT but it is very difficult to filter out the eclipse generated WLS from day-night terminator transition (TT) generated due to the fact that the eclipse occurred very close to TT which is the strong source of WLS. There was an intense geomagnetic storm ($Dst = -108$ nT) with main phase during 13/14 November 2012, but we do not see any WLS corresponding to storm activity during the period of our analysis shown in Figure 8 which is consistent with results of *Kumar et al*. [2015]. However, based on this analysis comparatively for shorter period of about 6 h (Figure 8), we cannot completely rule out the occurrence of WLS associated with storms as already reported by *Vlasov et al*. [2011, and references therein]. This could be our separate work by taking several intense storms with longer duration analysis mainly during the recovery phase of the storms. For the 9–10 May 2013 SE event, WLS on NPM signal were observed by ~ 85 min later than the eclipse shadow starting at Suva, whereas cooling spot intercepted the NPM-Suva TRGCP about 2 h later than SE shadow touching Suva station. Both NPM transmitter and Suva had almost the same eclipse magnitude and solar obscuration. The eclipse ended at ~2:00 UT at Suva, whereas it was maximum at NPM ~10 min before this time. Eclipse moved away from Suva at 02:00 UT, and WLS disappeared after ~02:40 UT, but there was partial eclipse at NPM. Above arguments indicate that a sudden change in the solar radiation apart from cooling spot could also generate the WLS which can appear after some time delay but not necessarily to remain present during all the time of SE on TRGCP. The observed WLS wave period in this study and the SE ionospheric response time are in the range of wave period generally between 20 and 60 min as reported in many previous ionospheric observations during eclipse using various techniques [*Altadill et al*., 2001; *Saulia et al*., 2007; *Chen et al*., 2011; *Ratnam et al*., 2012; *Yadav et al*., 2013]. However, the WLS time delays (on hour scale) as also found by *Maurya et al*. [2014] are significantly larger than *D* region ionospheric response time (~4–10 min) to SEs [*Lynn*, 1981; *Clilverd et al*., 2001]. The WLS time delays are different for different SEs which could be due to difference in the atmosphere cooling and velocity of AGWs associated with SEs. For 9–10 May 2013 annular SE, the occurrence time of WLS (00:00 UT, 10 May), eclipse commencement at Suva (22:40 UT, 9 May), interaction time of cooling spot with NPM-Suva TRGCP at about 01:35 UT on 10 May indicate that apart from the cooling spot the eclipse shadow can also excite the AGWs giving WLS detectable at *D* region heights. The range of WLS period (20–66 min) is maximum for 9–10 May 2013 annular SE and minimum (40–66 min) for 13–14 November 2012 total SE. The total interaction time of shadow and cooling spot with NPM-Suva TRGCP for 9–10 May annular SE was larger compared to 22 July 2009 total SE and 13–14 November 2012 total SE. This shows that range of WLS period apart from the distance between the cooling spot interaction with transmitter paths from station (*Maurya et al*. [2014] and relevant references) may also depend upon interaction time of SE with TRGCP. No significant change in the period and intensity of WLS is seen with the type and magnitude of SEs (Table 1 and Figure 8). As suggested by *Chimonas and Hines* [1970] and followed by *Maurya et al*. [2014], the WLS reported here are most probably due to electron density and temperature gradients created by blockage of *D* region ionization/solar flux superimposed with AGWs produced at various altitude due to differential heating because of supersonic movement of the Moon's shadow. Our results indicate that despite the well-accepted mechanism of AGWs generation during eclipse as discussed by *Chimonas* [1970], the observation of WLS at a given station and for a given solar eclipse event may depend on various factors like eclipse time and local time at transmitter and receiver, the time difference

between two, TRGCP path length, direction of eclipse propagation, eclipse magnitude and obscuration, and geomagnetic conditions. The difference in WLS characteristics could be due to one SE event (13–14 November 2012) that occurred during morning around 10 h LT when the ionosphere is still in a developing stage and two SE events (22 July 2009 and 9–10 May 2013) around 14 h LT when the ionosphere is fully developed. Further studies using many eclipse events and various combinations of TRGCPs are suggested to understand this subject more clearly. Our intention in this work is to find out the variation in the occurrence of WLS during different eclipses.

5. Conclusions

The LWPC modeling of the *D* region ionosphere during three eclipses (total SE of July 2009 and 13–14 November 2012 and annular SE of May 2013) observed at Suva, Fiji, a low-latitude station in the South Pacific region, showed moderate (0.5–1.5 km) increase in average VLF reference height with a maximum of 1.5 km for July 2009 total SE. The decrease in electron density for both total SEs by 25–32% is larger than of about 16% for annular SE of May 2013. Annular SE of May 2013 along with amplitude decrease also showed a systematic and good decrease in phase by 90° which gives $\alpha_{\text{eff}} = 6.86 \times 10^{-7} \text{cm}^{-3} \text{s}^{-1}$ at 75 km which is larger than eclipse time value of $\alpha_{\text{eff}} = 5 \times 10^{-7}\ \text{cm}^{-3}\ \text{s}^{-1}$ reported in the literature. Under the application of filter output of 20–80 min, the WLS of periods 24–60 min, 40–66 min, and 20–66 min associated with 22 July 2009, 13–14 November 2012, and 9–10 May 2013 have been estimated. The results indicate that SE-induced AGWs perturbed the *D* region ionosphere and induced the periodic variations in the electron density and hence in signal amplitude manifested through the wavelet analysis of signal amplitude. The occurrence of WLS for 9–10 May 2013 SE event on NPM signal before cooling spot interception with the NPM-Suva path shows that apart from SE cooling spot even the sudden changes in the solar radiation over path can also produce WLS. The periodicity and intensity of WLS did not show any clear dependence on the type and magnitude of SE indicating that they may also depend on various conditions such as time of SE occurrence time, TRGCP length, signal power, the background of atmosphere and ionosphere at the time of SE, and other geophysical and meteorological conditions which are never same for any two SEs. The results provide initial understanding on the dependence of SE-generated WLS on the TRGCP geometry. The detailed study on this topic is suggested as future work considering more eclipses intercepting various TRGCPs.

Acknowledgments
The authors of the University of the South Pacific sincerely thank Research Committee of Faculty of Science, Technology and Environment for financial support under staff project grant to carry out this work and World-Wide Lightning Location Network (www.wwlln.net) for providing lightning data. The information about SEs can be found in http://eclipse.gsfc.nasa.gov/SEmono/TSE2012/TSE2012.html and VLF transmitter data are available with the corresponding author. Ajeet Maurya thanks United States India Educational Foundation (USIEF) (award 2040/FNPDR/2015) New Delhi for Fulbright Nehru Postdoctoral Fellowship to carry out research at Georgia Tech Atlanta, USA.

References

Afraimovich, E. L., K. S. Palamartchouk, N. P. Perevalova, V. V. Chernukhov, A. V. Lukhnev, and V. T. Zalutsky (1998), Ionospheric effects of the solar eclipse of March 9, 1997, as deduced from the GPS data, *Geophys. Res. Lett.*, *25*(4), 465–468, doi:10.1029/98GL00186.

Afraimovich, E. L., et al. (2013), A review of GPS/GLONASS studies of the ionospheric response to natural and anthropogenic processes and phenomena, *J. Space Weather Space Clim.*, *3*, A27, doi:10.1051/swsc/2013049.

Altadill, D., J. G. Sole, and E. M. Apostolov (2001), Vertical structure of a gravity wave like oscillation in the ionosphere generated by the solar eclipse of August 11, 1999, *J. Geophys. Res.*, *106*(A10), 21,419–21,428, doi:10.1029/2001JA900069.

Anderson, R. C., D. R. Keefer, and O. E. Myers (1972), Atmospheric pressure and temperature changes during the 7 March 1970 solar eclipse, *J. Atmos. Sci.*, *29*, 583–587, doi:10.1175/1520-0469.

Antonia, R. A., A. J. Chambers, D. Phong-Anant, S. Rajagopalan, and K. R. Sreenivasan (1979), Response of atmospheric surface layer turbulence to a partial solar eclipse, *J. Geophys. Res.*, *4*, 1689–1692, doi:10.1029/JC084iC04p01689.

Baran, L. W., I. I. Ephishov, I. I. Shagimuratov, V. P. Ivanov, and A. F. Lagovsky (2003), The response of the ionospheric total electron content to the solar eclipse on 11 August 1999, *Adv. Space Res.*, *31*(4), 989–994, doi:10.1016/S0273-1177(02)00885-2.

Belrose, J. S., L. R. Bode, and L. W. Hewitt (1964), Physical properties of the polar winter mesosphere obtained from low-frequency propagation and partial reflection studies, *Radio Sci.*, *68D*, 1219–1323, doi:10.6028/jres.068D.136.

Chandra, H., S. Sharma, P. D. Lele, G. Rajaram, and A. Hanchinal (2007), Ionospheric measurements during the total solar eclipse of 11 August 1999, *Earth Planets Space*, *59*, 59–64, doi:10.1186/BF03352023.

Chen, G., Z. Zhao, Y. Zhang, G. Yang, C. Zhou, S. Huang, T. Li, N. Li, and H. Sun (2011), Gravity waves and spread *Es* observed during the solar eclipse of 22 July 2009, *J. Geophys. Res.*, *116*, A09314, doi:10.1029/2011JA016720.

Cheng, K., Y.-N. Huang, and S.-N. Chen (1992), Ionospheric effects of the solar eclipse of September 23, 1987, around the equatorial anomaly crest region, *J. Geophys. Res.*, *97*(A1), 103–111, doi:10.1029/91JA02409.

Chimonas, G. (1970), Internal gravity-wave motion induced in the Earth's atmosphere by a solar eclipse, *J. Geophys. Res.*, *75*(28), 5545–5551, doi:10.1029/JA075i028p05545.

Chimonas, G., and C. O. Hines (1970), Atmospheric gravity waves induced by a solar eclipse, *J. Geophys. Res.*, *75*, 857–875, doi:10.1029/JA075i004p00875.

Chuo, Y. J. (2013), Ionospheric effects on the *F* region during the sunrise for the annular solar eclipse over Taiwan on 21 May 2012, *Ann. Geophys.*, *31*, 1891–1898, doi:10.5194/angeo-31-1891-2013.

Clilverd, M. A., C. J. Rodger, N. R. Thomson, J. Lichtenberger, P. Steinbach, P. Cannon, and M. J. Angling (2001), Total solar eclipse effects on VLF signals: Observation and modeling, *Radio Sci.*, *36*(4), 773–788, doi:10.1029/2000RS002395.

Cummer, S. A., and U. S. Inan (2000), Ionospheric *E* region remote sensing with ELF radio atmospherics, *Radio Sci.*, *35*, 1437–1444, doi:10.1029/2000RS002335.

Curto, J. J., B. Heiig, and M. Pinol (2006), Modeling the geomagnetic effects caused by solar eclipse of 11 August 1999, *J. Geophys. Res.*, *111*, A07312, doi:10.1029/2005JA011499.
Gerasopoulos, E., et al. (2008), The total solar eclipse of March 2006: Overview, *Atmos. Chem. Phys.*, *8*, 5205–5220, doi:10.5194/acp-8-5205-2008.
Grubor, D., and D. Šulić (2002), Signal strength response to 11 August 1999 eclipse effect on *D* region, *Proc. URSI*. [Available at www.ursi.org/Proceedings/ProcGA02/papers/p1293.pdf.]
Guha, A., B. K. De, R. Roy, and A. Choudhury (2010), A response of the equatorial lower ionosphere to the total solar eclipse of 22 July 2009 during sunrise transition period studied using VLF signal, *J. Geophys. Res.*, *115*, A11302, doi:10.1029/2009JA015101.
Hargreaves, J. K. (1992), *The Solar-Terrestrial Environment*, Cambridge Univ. Press, New York.
Kaladze, T. D., O. A. Pokhotelov, H. A. Shah, M. I. Khan, and L. Stenflo (2008), Acoustic-gravity waves in the Earth's ionosphere, *J. Atmos. Sol. Terr. Phys.*, *70*, 1607–1616, doi:10.1016/j.jastp.2008.06.009.
Kato, S., T. Kawakami, and D. John (1977), Theory of gravity wave emission from moving sources in the upper atmosphere, *J. Atmos. Sol. Terr. Phys.*, *39*, 581–588, doi:10.1016/0021-9169(77)90067-8.
Kumar, A., and S. Kumar (2014), Space weather effects on the low latitude *D* region ionosphere during solar minimum, *Earth Planet. Space*, *66*, 76–86, doi:10.1186/1880-5981-66-76.
Kumar, S., A. Kumar, F. Menk, A. K. Maurya, R. Singh, and B. Veenadhari (2015), Response of the low-latitude *D* region ionosphere to extreme space weather event of 14–16 December 2006, *J. Geophys. Res. Space Physics*, *120*, 788–799, doi:10.1002/2014JA020751.
Laštovička, J. (2009), Lower ionosphere response to external forcing: A brief review, *Adv. Space Res.*, *43*, 1–14, doi:10.1016/j.asr.2008.10.001.
Lynn, K. J. W. (1981), The total solar eclipse of 23 October 1976, observed at VLF, *J. Atmos. Sol. Terr. Phys.*, *43*, 1309–1316, doi:10.1016/0021-9169(81)90156-2.
Maurya, A. K., D. V. Phanikumar, R. Singh, S. Kumar, B. Veenadhari, Y.-S. Kwak, A. Kumar, A. K. Singh, and K. Niranjan Kumar (2014), Low-mid latitude *D* region ionospheric perturbations associated with 22 July 2009 total solar eclipse: Wave-like signatures inferred from VLF observations, *J. Geophys. Res. Space Physics*, *119*, 8512–8523, doi:10.1002/2013JA019521.
McRae, W. M., and N. R. Thomson (2000), VLF phase and amplitude: Daytime ionospheric parameters, *J. Atmos. Sol. Terr. Phys.*, *62*(7), 09–618, doi:10.1016/S1364-6826(00)00027-4.
McRae, W. M., and N. R. Thomson (2004), Solar flare induced ionospheric *D* region enhancements from VLF phase and amplitude observations, *J. Atmos. Sol. Terr. Phys.*, *66*, 77–87, doi:10.1016/j.jastp.2003.09.009.
Mitra, A. P. (1968), A review of *D* region processes in non-polar latitudes, *J. Atmos. Sol. Terr. Phys.*, *30*, 1065–1114.
Mitra, A. P. (1974), Ionospheric effects of solar flares, in *Astrophysics and Space Science Library*, vol. 46, D. Reidel Comp., Boston, Mass.
Molchanov, O. A., and M. Hayakawa (2008), *Seismo Electromagnetics and Related Phenomena: History and Latest Results*, 189 pp., TERRAPUB, Tokyo.
Nina, A., and V. M. C˘adze (2013), Detection of acoustic-gravity waves in lower ionosphere by VLF radio waves, *Geophys. Res. Lett.*, *40*, 4803–4807, doi:10.1002/grl.50931.
Ohya, H., F. Tsuchiya, H. Nakata, K. Shiokawa, Y. Miyoshi, K. Yamashita, and Y. Takahashi (2012), Reflection height of daytime tweek atmospherics during the solar eclipse of 22 July 2009, *J. Geophys. Res.*, *117*, A11310, doi:10.1029/2012JA018151.
Pal, S., S. K. Chakrabarti, and S. K. Mondal (2012), Modeling of sub-ionospheric VLF signal perturbations associated with total solar eclipse, 2009 in Indian subcontinent, *Adv. Space Res.*, *50*, 196–204, doi:10.1016/j.asr.2012.04.007.
Peter, W. B., M. W. Chevalier, and U. S. Inan (2006), Perturbations of midlatitude subionospheric VLF signals associated with lower ionospheric disturbances during major geomagnetic storms, *J. Geophys. Res.*, *111*, A03301, doi:10.1029/2005JA011346.
Phanikumar, D. V., Y.-S. Kwak, A. K. Patra, A. K. Maurya, R. Singh, and S.-M. Parke (2014), Response of the mid-latitude *D* region ionosphere to the total solar eclipse of 22 July 2009 studied using VLF signals in South Korean peninsula, *Adv. Space Res.*, *54*, 961–968, doi:10.1016/j.asr.2014.06.005.
Ratnam, M. V., S. Eswaraiah, P. P. Leena, A. K. Patra, B. V. KrishnaMurthy, and S. V. B. Rao (2012), Effect of the annular solar eclipse of 15 January 2010 on the low latitude mesosphere, *J. Atmos. Sol. Terr. Phys.*, *80*, 340–346, doi:10.1016/j.jastp.2012.02.022.
Sauli, P., P. Abry, P. Boska, and L. Duchayne (2006), Wavelet characterization of ionospheric acoustic and gravity waves occurring during solar eclipse of August 11, 1999, *J. Atmos. Sol. Terr. Phys.*, *68*, 586–598, doi:10.1016/j.jastp.2005.03.024.
Saulia, P., S. G. Rouxb, P. Abryb, and J. Boska (2007), Acoustic–gravity waves during solar eclipses: Detection and characterization using wavelet transforms, *J. Atmos. Sol. Terr. Phys.*, *69*, 2465–2484, doi:10.1016/j.jastp.2007.06.012.
Singh, L., et al. (1989), Mulit-station satellite radio beacon study of ionospheric variations during total solar eclipses, *J. Atmos. Sol. Terr. Phys.*, *51*, 271–278, doi:10.1016/0021-9169(89)90078-0.
Singh, R., B. Veenadhari, A. K. Maurya, M. B. Cohen, S. Kumar, R. Selvakumaran, P. Pant, A. K. Singh, and U. S. Inan (2011), *D* region ionosphere response to the total solar eclipse of 22 July 2009 deduced from ELF-VLF tweek observations in the Indian sector, *J. Geophys. Res.*, *116*, A10301, doi:10.1029/2011JA016641.
Thomson, N. R. (1993), Experimental daytime VLF ionospheric parameters, *J. Atmos. Sol. Terr. Phys.*, *55*, 173–184, doi:10.1016/0021-9169(93).
Thomson, N. R., C. J. Rodger, and M. A. Clilverd (2005), Large solar flares and their ionospheric *D* region enhancements, *J. Geophys. Res.*, *110*, A06306, doi:10.1029/2005JA011008.
Todoroki, Y., S. Maekawa, T. Yamauchi, T. Horie, and M. Hayakawa (2007), Solar flare induced *D* region perturbation in the ionosphere, as revealed from a short-distance VLF propagation path, *Geophys. Res. Lett.*, *34*, L03103, doi:10.1029/2006GL028087.
Vlasov, A., K. Kauristie, M. van de Kamp, J.-P. Luntama, and A. Pogoreltsev (2011), A study of traveling ionospheric disturbances and atmospheric gravity waves using EISCAT Svalbard radar IPY-data, *Ann. Geophys.*, *29*, 2101–2116, doi:10.5194/angeo-29-2101-2011.
Wait, J. R., and K. P. Spies (1964), Characteristics of the Earth-ionosphere waveguide for VLF radio waves, *Tech. Note 300*, Natl. Bur. of Stand., Boulder, Co.
Walker, G. O., T. Y. Y. Li, Y. W. Wong, T. Kikuchi, and Y. N. Huang (1991), Ionospheric and geomagnetic effects of the solar eclipse of 18 March 1988 in East-Asia, *J. Atmos. Sol. Terr. Phys.*, *53*, 25–3, doi:10.1016/0021-9169(91)90017-2.
Yadav, S., R. M. Das, R. S. Dabas, and A. K. Gwal (2013), The response of sporadic *E*-layer to the total solar eclipse of July 22, 2009 over the equatorial ionization anomaly region of the Indian zone, *Adv. Space Res.*, *51*, 2043–2047, doi:10.1016/j.asr.2013.01.011.
Zhang, X., Z. Zhao, Y. Zhang, and C. Zhou (2010), Observations of the ionosphere in the equatorial region using WISS during total solar eclipse of 22 July 2009, *J. Atmos. Sol. Terr. Phys.*, *72*, 869–875, doi:10.1016/j.jastp.2010.04.012.
Zhang, X.-F., R. Y. Du, S.-M. Gu, T. Wu, and Y.-N. Wang (2011), Anomalous variation of VLF signals in the total solar eclipse of 22 July 2009, *Chin. Astron. Astrophys.*, *35*, 54–61.